

Inverse Design of Ultralow Lattice Thermal Conductivity Materials Via Lone Pair Cation Coordination Environment

Eric B. Isaacs,[†] Grace M. Lu,^{†,‡} and Christopher Wolverton^{*,†}

[†]*Department of Materials Science and Engineering, Northwestern University, Evanston, Illinois 60208, USA*

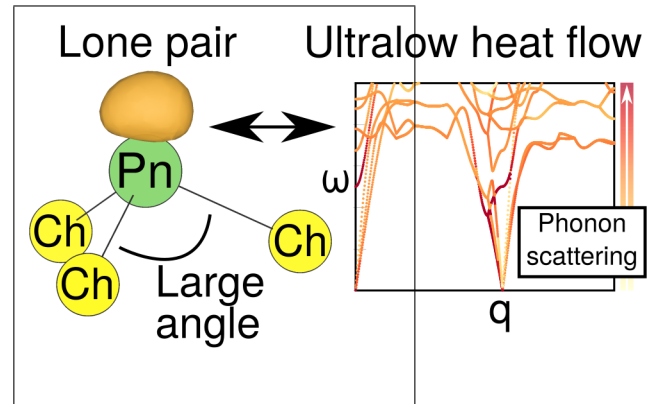
[‡]*Present Address: Department of Materials Science and Engineering, University of Illinois at Urbana-Champaign, Urbana, IL 61801, USA*

E-mail: c-wolverton@northwestern.edu

Abstract

The presence of lone pair (LP) electrons is strongly associated with the disruption of lattice heat transport, which is a critical component of strategies to achieve efficient thermoelectric energy conversion. By exploiting an empirical relationship between lattice thermal conductivity κ_L and the bond angles of pnicogen group LP cation coordination environments, we develop an inverse design strategy based on a materials database screening to identify chalcogenide materials with ultralow κ_L for thermoelectrics. Screening the $\sim 635,000$ real and hypothetical inorganic crystals of the Open Quantum Materials Database based on the constituent elements, nominal electron counting, LP cation coordination environment, and synthesizability, we identify 189 compounds expected to exhibit ultralow κ_L . As a validation, we explicitly compute the lattice dynamical properties of two of the compounds ($\text{Cu}_2\text{AgBiPbS}_4$ and $\text{MnTl}_2\text{As}_2\text{S}_5$) using first-principles calculations and successfully find both achieve ultralow κ_L values at room temperature of $\sim 0.3\text{--}0.4$ W/(m·K) corresponding to the amorphous limit. Our data-driven approach provides promising candidates for thermoelectric materials and opens new avenues for the design of phononic properties of materials.

Graphical TOC Entry



Minimizing lattice thermal transport is critical for thermoelectric heat-to-electricity conversion, in which such heat flow acts as a loss mechanism.¹ This can be seen in the dimensionless thermoelectric figure of merit to be maximized

$$ZT = \frac{\sigma S^2}{\kappa_L + \kappa_e} T,$$

in which the lattice thermal conductivity κ_L appears in the denominator. Here, σ is electrical conductivity, κ_e is electronic thermal conductivity (typically small in semiconductors), S is thermopower, and T is temperature. Achieving ultralow values of κ_L [i.e., $\lesssim 1$ W/(m·K)] is an integral component of successful strategies to design high-performance thermoelectric materials.²

While there exist various strategies to extrinsically reduce κ_L , such as nanostructuring, alloying, and doping (see, e.g., Refs. 3–13), a conceptually appealing alternative approach is to instead utilize materials with intrinsically ultralow κ_L .¹⁴ One characteristic related to ultralow κ_L in certain materials is the presence of a lone pair (LP), a pair of valence electrons localized on a single atom.¹⁵ A LP is typically achieved via a cation (called a LP cation) whose two valence s electrons remain localized on or near the cation. For example, given Sn's electronic configuration of [Kr] $4d^{10} 5s^2 5p^2$, Sn^{2+} (as in SnSe) is a LP cation, whereas Sn^{4+} (as in SnSe_2) is not. Elements commonly forming LP cations include elements in group III (Tl; 1+ oxidation state), group IV (Ge, Sn, Pb; 2+ oxidation state), and the pnictogen group (P, As, Sb, Bi; 3+ oxidation state) of the periodic table.^{16–20}

It has been long known that the presence of LP cations is related to low thermal conductivity. In 1961, Petrov and Shtrum observed that thermal conductivity values of $\text{A}^{\text{I}}\text{B}^{\text{V}}\text{X}_2^{\text{VI}}$ compounds (whose B^{3+} is a LP cation) are significantly lower than those of $\text{A}^{\text{I}}\text{B}^{\text{III}}\text{X}_2^{\text{VI}}$ compounds (whose B^{3+} is not a LP cation), where A^{I} , B^{III} , and B^{V} are monovalent, trivalent, and pentavalent elements, respectively, and X^{VI} is a chalcogen.²¹ For example, room-temperature κ_L for AgSbSe_2 is only 0.7 W/(m·K), as com-

pared to 1.8 W/(m·K) for AgInSe_2 .²² Similarly, room-temperature κ_L for Cu_3SbSe_4 (whose Sb^{5+} is not a LP cation) is 2.5–3.5 W/(m·K), much larger than the corresponding 0.7–1.0 W/(m·K) for Cu_3SbSe_3 (whose Sb^{3+} is a LP cation), despite the two compounds containing the same elements and having similar stoichiometry.^{23,24} Therefore, it is not surprising that several of the most promising thermoelectrics (e.g., PbTe, Bi_2Te_3 , and SnSe) contain LP cations and that many other compounds containing LP cations have also been under investigation.^{25–32}

Empirically, the coordination environment of a LP cation was found by Skoug and Morelli to be intimately related to lattice thermal transport.³³ In particular, within a set of compounds containing pnictogen group lone pair cations (L) coordinated to a given number of chalcogens (X), e.g., compounds whose L have 3 nearest neighbor X atoms, they observed a strong negative correlation between measured room-temperature κ_L and a local structural parameter related to the bond angles $\angle\text{X-L-X}$ of the LP cation's coordination cage. This parameter $\bar{\alpha}^{(s)}$ can be defined as

$$\bar{\alpha}^{(s)} = \frac{1}{N_{\text{ang}}^{(s)}} \sum_i \alpha_i^{(s)} \theta(\alpha_{\text{max}} - \alpha_i^{(s)}),$$

where $\alpha_i^{(s)}$ is the i^{th} $\angle\text{X-L-X}$ for the s^{th} LP cation site, θ is the Heaviside step function, α_{max} is $\cos^{-1}(-\frac{1}{3}) \approx 109.5^\circ$ (bond angle for ideal tetrahedral coordination), and $N_{\text{ang}}^{(s)} = \sum_i \theta(\alpha_{\text{max}} - \alpha_i^{(s)})$. In words, $\bar{\alpha}^{(s)}$ is simply the average of the $N_{\text{ang}}^{(s)}$ bond angles no larger than 109.5° for the s^{th} LP cation site. The quantity $\bar{\alpha}^{(s)}$, which originates from a study of Sb chalcogenides using the bond valence sum concept, was found to relate to the effective valence of the LP cation (i.e., between the nominal 3+ and 5+ common oxidation states for Sb) and was interpreted as describing the retraction of the LP from the LP cation.³⁴ In general, the work of Skoug and Morelli (and others³⁵) strongly suggests the importance of the LP cation environment and spatial distribution of the LP in influencing lattice dynamics.

In this Letter, we exploit the connection between LP cation coordination environment and lattice heat transport with the goal of designing ultralow κ_L materials. We develop an inverse design approach based on a materials database screening, which can be considered the so-called “second modality” of inverse design³⁶ and is related to our previous works on inverse design for electronic band structure.^{37,38} Searching for synthesizable compounds containing pnictogen group LP cations coordinated to chalcogens with large $\bar{\alpha}^{(s)}$ (corresponding to low κ_L), we identify 189 compounds. As a validation, we explicitly compute the lattice dynamical properties for two of the identified compounds, $\text{Cu}_2\text{AgBiPbS}_4$ and $\text{MnTl}_2\text{As}_2\text{S}_5$, and successfully find ultralow κ_L values of $\sim 0.3\text{--}0.4$ W/(m·K) at room temperature. In addition to providing promising ultralow κ_L materials, our data-driven approach opens up new avenues for inverse design of lattice dynamical properties.

Our design space consists of the materials within the Open Quantum Materials Database (OQMD),^{39,40} which contains electronic structure calculations based on density functional theory (DFT)^{41,42} for $\sim 635,000$ (as of November 2019) known and hypothetical inorganic crystals derived from the Inorganic Crystal Structure Database (ICSD)^{43,44} and structural prototypes. Our initial screening, before taking into account $\bar{\alpha}^{(s)}$, is based on several criteria that must be simultaneously satisfied:

1. **Chemical elements** – Compound must contain one or more of the pnictogen group elements that commonly occur with a 3+ oxidation state (As, Sb, Bi), one or more chalcogen elements (S, Se, Te), and (for practicality) no radioactive elements.
2. **Electron count** – The pnictogen must have an oxidation state of 3+ (so it is a LP cation) and all other elements must have integer oxidation states (to focus on possible semiconductors/insulators).
3. **Crystal structure** – Each pnictogen atom must be coordinated solely by chalcogen atoms and must have a coordination number ≥ 3 .
4. **Synthesizability** – The compound formation energy must be at most 25 meV/atom above that of the thermodynamic ground state determined by convex hull analysis (consistent with the overall scale of metastability for experimentally observed chalcogenides⁴⁵) and/or reported experimentally. This criterion is chosen to focus on synthesizable compounds.

The criteria are based on pnictogen group LP cations (as opposed to others like Pb^{2+} and Tl^+) and chalcogens since the data in work of Skoug and Morelli pertain to such chemistries. Further details about the screening criteria are included in the Supporting Information.

352 compounds pass the initial screening criteria. Although we have characterized these compounds in terms of chemical composition, crystal structure, electronic properties, and synthesizability (see the Supporting Information), we focus here on the local coordination environment of the LP cations. Fig. 1(a) shows the coordination number and $\bar{\alpha}^{(s)}$ of each pnictogen LP cation element in the 352 compounds. For atomic sites with complex, low-symmetry coordination environments (often the case for LP cations), defining coordination number can be challenging. Therefore, to avoid ambiguity, we employ the well-defined effective coordination number of Hoppe,⁴⁶ a continuous quantity that includes contributions (smoothly and rapidly decaying with increasing distance) from all other atoms. For compounds containing multiple sites of a LP cation element with distinct environments, we show the average values of coordination number and $\bar{\alpha}^{(s)}$ (which we call $\langle \text{CN} \rangle$ and $\langle \bar{\alpha} \rangle$, respectively), with the ranges indicated by the “error bars.” The coordination number generally increases as the LP cation element goes down the pnictogen group of the periodic table (As \rightarrow Sb \rightarrow Bi). In addition, consistent with the work of Skoug and Morelli, we generally find smaller $\bar{\alpha}^{(s)}$ values for larger coordination number.³³ Notably, many of the 352 compounds exhibit large $\bar{\alpha}^{(s)}$ values $\sim 90\text{--}100^\circ$.

To search for the most promising compounds, we further screen based on $\bar{\alpha}^{(s)}$. Since the

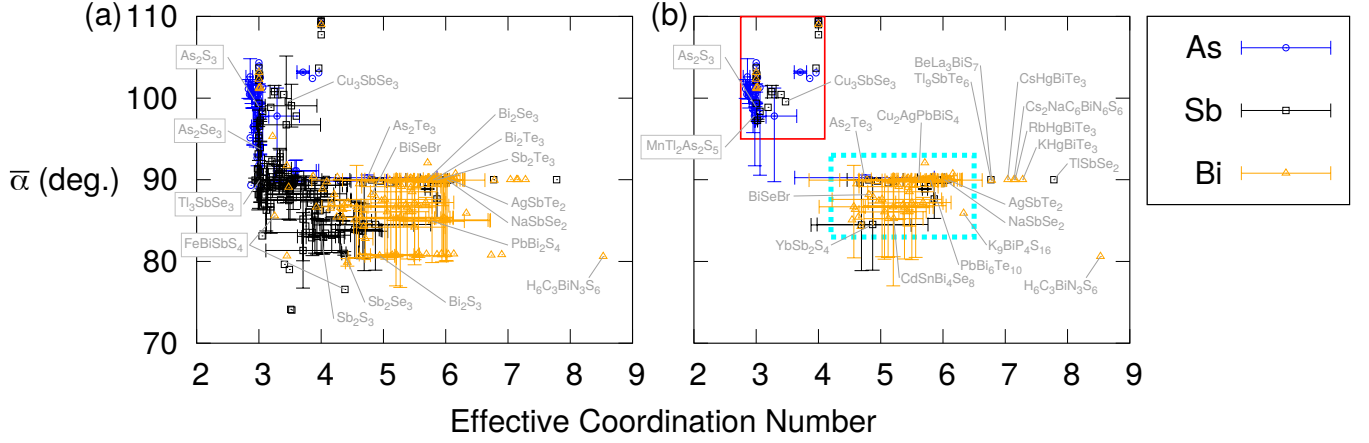


Figure 1: Coordination number and $\bar{\alpha}^{(s)}$ for each pnictogen LP cation element in the (a) 352 compounds passing our initial screening criteria and (b) 189 (of the 352) compounds also with promising coordination environment, as discussed in the main text. Points correspond to average (over LP cation sites) values and the “error bars” indicate the ranges. A variety of data points are labeled with the compound composition to give a general sense for the compounds identified. In panel (b), the solid red and dotted cyan rectangles show two distinct regions, discussed in the main text, containing a vast majority of the compounds.

work of Skoug and Morelli suggests the need for large $\bar{\alpha}^{(s)}$ relative to typical values for LP cations of similar coordination number, we retain a compound if one or more of its pnictogen LP cation elements is suitable in this sense. Specifically, for the combination of compound and constituent pnictogen LP cation element under consideration, its $\langle \bar{\alpha} \rangle$ must be no more than 7% smaller than the “best” value, which we take to be the maximum value in the following set: $\langle \bar{\alpha} \rangle$ for all combinations of compound and constituent LP cation element whose $\langle \text{CN} \rangle$ differs by no more than 0.5 from the one under consideration. For example, Bi in FeBiSbS_4 ($\langle \text{CN} \rangle = 3.25$, $\langle \bar{\alpha} \rangle = 85.6^\circ$) does not satisfy this criterion since 85.6° is more than 7% smaller than the largest $\langle \bar{\alpha} \rangle$ value in the $2.75 \leq \langle \bar{\alpha} \rangle \leq 3.75$ region of Fig. 1(a). Since Sb in FeBiSbS_4 also does not satisfy its corresponding criterion, FeBiSbS_4 is discarded. The specific critical value employed (7%) is fairly arbitrary and is simply chosen to reduce the number of compounds by around a factor of two.

189 of the 352 compounds, whose coordination number and $\bar{\alpha}^{(s)}$ are shown in Fig. 1(b), pass this additional screening criterion. The majority of the compounds occur in two regions: (1) the red region of smaller coordi-

ination number (containing many As compounds) and (2) the cyan region of larger coordination number (containing many Bi compounds). The 189 compounds we have identified should be considered promising candidates for ultralow κ_L , and possibly thermoelectric applications. Indeed, among the 189 are various systems that have been explored previously for thermoelectricity and exhibit low κ_L , such as AgBiS_2 ,⁴⁷ AgBi_3S_5 ,^{48,49} Bi_2Se_3 ,^{50–52} $\text{K}_2\text{Bi}_8\text{Se}_{13}$,⁵³ AgBiSe_2 ,^{22,54} Bi_2Te_3 ,^{52,55} $\text{Bi}_2\text{Te}_2\text{Se}$,^{52,56} AgBiTe_2 ,^{57,58} GeBi_2Te_4 ,^{59,60} GeBi_4Te_7 ,^{60–62} PbBi_2Te_4 ,^{59,62} PbBi_4Te_7 ,^{59,62} Tl_9BiTe_6 ,^{63–66} Cu_3SbSe_3 ,^{33,67,68} AgSbTe_2 ,^{22,69,70} TlSbTe_2 ,^{65,71} and Tl_9SbTe_6 .⁶⁶

In order to validate our approach, we explicitly compute the lattice thermal transport behavior for two of the identified compounds. We choose one compound from the cyan region ($\text{Cu}_2\text{AgBiPbS}_4$) and one from the red region ($\text{MnTl}_2\text{As}_2\text{S}_5$) of Fig. 1(b). Both compounds exist (i.e., they are experimental structures from the ICSD), but they have not been explored for thermoelectricity. We note that they are metastable compounds within the OQMD whose formation energies are a small amount (13–14 meV/atom) above the convex hull.

Fig. 2 shows the crystal structures of

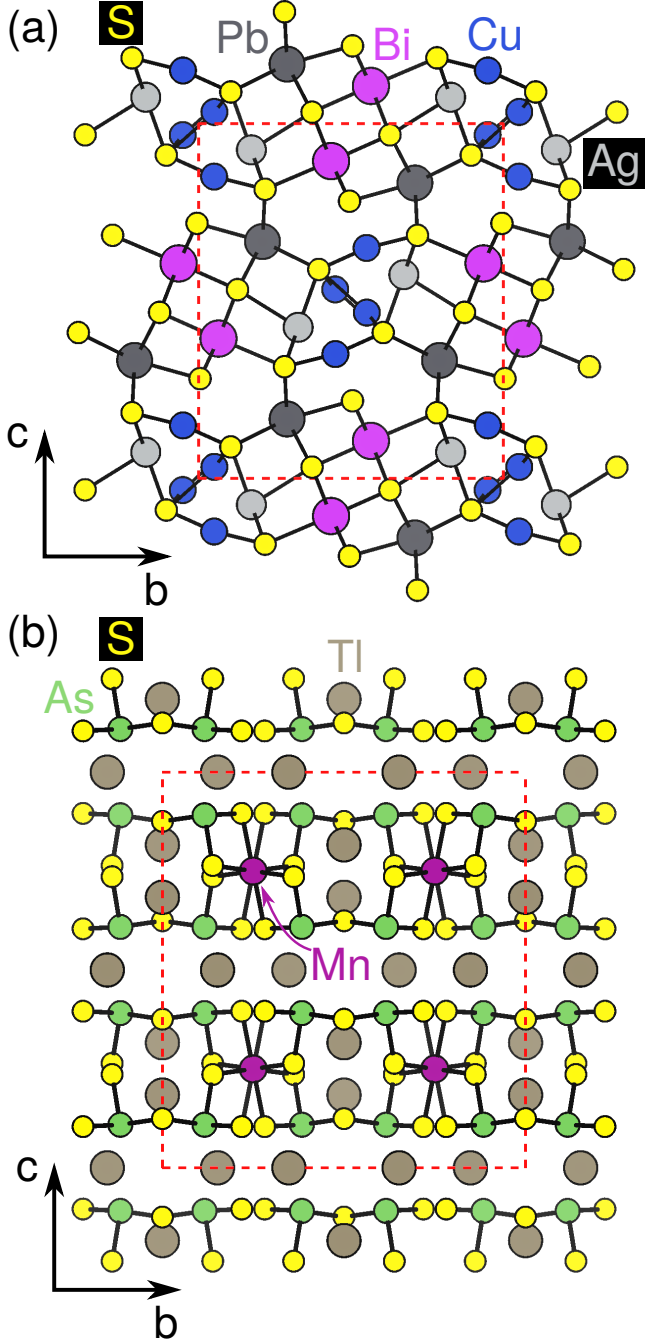


Figure 2: Crystal structures of (a) $\text{Cu}_2\text{AgBiPbS}_4$ and (b) $\text{MnTl}_2\text{As}_2\text{S}_5$. The unit cell is shown as the dashed red line.

$\text{Cu}_2\text{AgBiPbS}_4$ and $\text{MnTl}_2\text{As}_2\text{S}_5$. $\text{Cu}_2\text{AgBiPbS}_4$, a mineral, is orthorhombic ($Pnma$ space group) with a complex 3D bonding network.⁷² In $\text{Cu}_2\text{AgBiPbS}_4$, Bi^{3+} is octahedral with $\langle\bar{\alpha}\rangle = 89.98^\circ$ and $\langle\text{CN}\rangle = 5.61$, whereas Cu^+ exists in linear and trigonal planar coordinations, Ag^+ is trigonal pyramidal, and Pb^{2+} (also a LP cation) is capped trigonal prismatic. $\text{MnTl}_2\text{As}_2\text{S}_5$, which has been synthesized hydrothermally, also crystallizes with an orthorhombic ($Cmce$) space group, and it can be considered a layered structure.^{73,74} In $\text{MnTl}_2\text{As}_2\text{S}_5$, As^{3+} is trigonal pyramidal with $\langle\bar{\alpha}\rangle = 97.82^\circ$ and $\langle\text{CN}\rangle = 2.97$, Mn^{2+} is octahedral, and Tl^+ (also a LP cation) is square pyramidal.

Table 1: Group velocity v at Γ (in km/s), Debye temperature Θ (in K), and root-mean-square Grüneisen parameter for each acoustic branch in each direction.

$\text{Cu}_2\text{AgBiPbS}_4$			
	TA	TA'	LA
v_x	1.2	1.8	3.2
v_y	1.3	1.4	3.0
v_z	1.5	1.9	1.9
$\Theta_{\Gamma X}$	28	32	30
$\Theta_{\Gamma Y}$	21	21	25
$\Theta_{\Gamma Z}$	17	23	18
$\gamma_{\Gamma X}$	6.7	6.8	10.4
$\gamma_{\Gamma Y}$	3.1	1.6	5.2
$\gamma_{\Gamma Z}$	2.2	4.5	3.3
$\text{MnTl}_2\text{As}_2\text{S}_5$			
	TA	TA'	LA
v_x	1.2	1.5	2.2
v_y	1.4	1.8	2.7
v_z	1.1	1.3	2.2
$\Theta_{\Gamma X}$	33	26	33
$\Theta_{\Gamma Y}$	26	25	37
$\Theta_{\Gamma Z}$	13	16	16
$\gamma_{\Gamma X}$	2.4	2.4	2.2
$\gamma_{\Gamma Y}$	3.4	3.2	1.5
$\gamma_{\Gamma Z}$	22.5	6.4	2.8

We focus on lattice dynamical properties, but

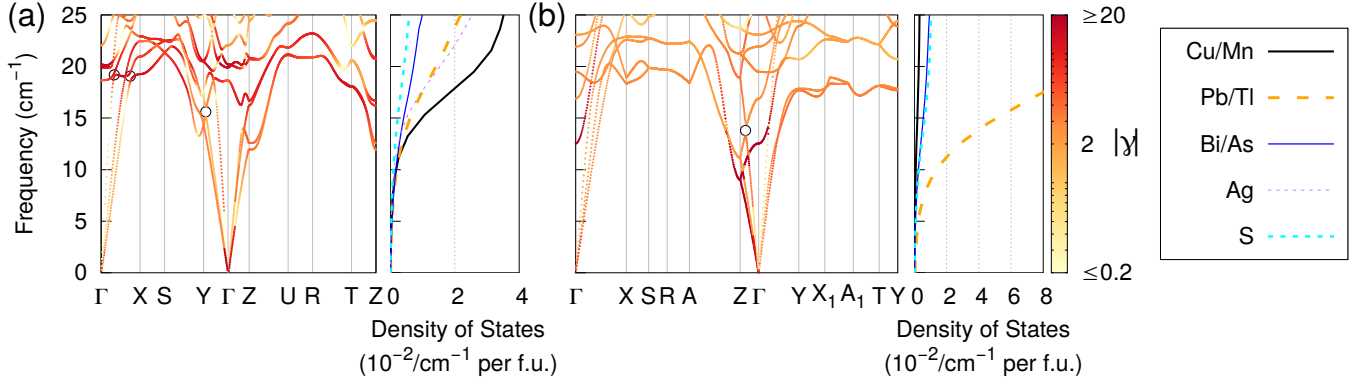


Figure 3: Low-frequency phonon dispersion and projected phonon density of states of (a) $\text{Cu}_2\text{AgBiPbS}_4$ and (b) $\text{MnTl}_2\text{As}_2\text{S}_5$. The line color indicates the magnitude of the mode Grüneisen parameter γ . Circles are shown at avoided crossings.

details on the electronic properties are included in the Supporting Information for completeness. The low-frequency phonon dispersions for $\text{Cu}_2\text{AgBiPbS}_4$ and $\text{MnTl}_2\text{As}_2\text{S}_5$ are shown in Fig. 3. Due to partial occupancy of the trigonal planar Cu site (not considered in the OQMD), we employ a unit cell doubled along the x direction to study $\text{Cu}_2\text{AgBiPbS}_4$, as discussed in detail in the Supporting Information. Both materials exhibit acoustic and optical phonons that are quite low in frequency. In the case of $\text{Cu}_2\text{AgBiPbS}_4$, vibrations of all four cations contribute appreciably to these modes, with Cu vibrations contributing the most. For $\text{MnTl}_2\text{As}_2\text{S}_5$, Tl vibrations are dominant. The computed sound velocities and Debye temperatures (taken to be the zone boundary frequencies) for each acoustic branch and direction are shown in Table 1. Both exhibit sound velocities of $\sim 1\text{--}3$ km/s and, due in part to the complexity of the unit cell, Debye temperatures of only $\sim 15\text{--}40$ K. Therefore, both $\text{Cu}_2\text{AgBiPbS}_4$ and $\text{MnTl}_2\text{As}_2\text{S}_5$ are very soft in terms of elastic (harmonic) properties.

To measure the anharmonicity in $\text{Cu}_2\text{AgBiPbS}_4$ and $\text{MnTl}_2\text{As}_2\text{S}_5$, we compute the mode Grüneisen parameter. Defined as $\gamma = -\frac{\partial\omega/\omega}{\partial V/V}$, where ω is phonon frequency and V is crystal volume, the Grüneisen parameter provides a measure of the strength of the phonon-phonon scattering, which limits lattice heat transport. As shown in Fig. 3 and Table 1, both compounds exhibit large Grüneisen parameter for

the acoustic and especially the low-lying optical modes. For example, for the optical modes, we find values of ~ -15 for $\text{Cu}_2\text{AgBiPbS}_4$ and ~ 20 for $\text{MnTl}_2\text{As}_2\text{S}_5$. For the $\text{MnTl}_2\text{As}_2\text{S}_5$ case, the lowest optical mode at the zone center contains substantial Tl motion. Therefore, especially given the large experimental atomic displacement parameters for Tl ($28\text{--}36 \times 10^{-3} \text{ \AA}^2$),⁷³ the concept of “rattler” Tl atoms^{75,76} may be relevant to $\text{MnTl}_2\text{As}_2\text{S}_5$. In contrast, for the $\text{Cu}_2\text{AgBiPbS}_4$ case, the lowest optical mode at the zone center corresponds to a collective motion of all atom types. Visualizations of various phonon modes are included in the Supporting Information.

Determining a highly accurate prediction of κ_L for complex crystals is a significant challenge and is outside the scope of this work. However, to establish a baseline estimate for the magnitude, we employ the Debye-Callaway model,^{77,78} which has been used to provide a good qualitative picture for a variety of low- κ_L materials.^{24,49,79–81} In this approach, for which the data in Table 1 serve as input, only acoustic phonon scattering is considered. Due to the soft elastic properties, complex unit cell, and substantial anharmonicity, the computed Debye-Callaway model κ_L values are only $0.01\text{--}0.03$ W/(m·K) for $\text{Cu}_2\text{AgBiPbS}_4$ and $0.01\text{--}0.07$ W/(m·K) for $\text{MnTl}_2\text{As}_2\text{S}_5$. Such low values, which can only result since the Debye-Callaway model does not consider that the interatomic distance is a lower bound to the phonon mean

free path, are below the minimum possible (amorphous limit) κ_L . Therefore, we take the minimum κ_L , via the Cahill model,⁸² as our best expectation for the measured lattice thermal conductivity. We find minimum κ_L of 0.44, 0.40, and 0.38 W/m·K in the x , y , and z directions, respectively, for $\text{Cu}_2\text{AgBiPbS}_4$. Similarly, we find minimum κ_L of 0.31, 0.38, and 0.29 W/m·K in the x , y , and z directions, respectively, for $\text{MnTl}_2\text{As}_2\text{S}_5$. Both compounds thus are expected to successfully achieve the desired ultralow κ_L , validating our approach.

Our inverse design strategy is successful in that we have identified materials (fully listed in the Supporting Information) very likely to exhibit the desired ultralow κ_L . A natural question is whether this success stems from solely a correlation between the properties of the LP and κ_L , or whether the relationship is causal. Previously, it has been proposed that the large polarizability of the LP does cause anharmonicity due to electrostatic interaction between the LP and the bonding states,^{21,24,33,83} As evidence, Zhang *et al.* observed that anharmonic phonon modes in Cu_3SbSe_3 involve motion of the Sb^{3+} in the direction of the LP,²⁴ and Nielsen *et al.* found that the Sb^{3+} LP is encompassed by the polarization response to Se atomic motion associated with anharmonic modes in NaSbSe_2 .⁸³ In addition, it has been argued that the further spatial removal of the LP from the LP cation in particular, as represented by large $\langle \bar{\alpha} \rangle$, enhances the anharmonicity.³³

Isolating the specific role of the LP in producing low κ_L remains a significant challenge.⁸⁴ To investigate this role for $\text{Cu}_2\text{AgBiPbS}_4$ and $\text{MnTl}_2\text{As}_2\text{S}_5$, we perform calculations to assess the coupling of the LP to the anharmonic phonon modes. As discussed in the Supporting Information, based on our analysis of the electronic localization function and electronic density of states, we do not find evidence for an especially strong coupling. In particular, we find no dramatic change in either the spatial location or the energy of the LP (which is far below the valence band edge in our case) as a result of the anharmonic phonons. As such, for the compounds in this study, we are unable to claim that the presence of the LP, or the specific

LP cation coordination environment or spatial distribution of the LP, directly causes the ultralow κ_L . In any case, our data-driven inverse design approach based on the established correlation between LP cation properties is capable of providing promising materials with ultralow κ_L and opens the door to future strategies for inverse design of phononic properties.

Computational Methods

DFT calculations using a plane-wave basis set and the projector augmented wave method^{85–87} are performed using VASP.⁸⁸ We employ the generalized gradient approximation of Perdew, Burke, and Ernzerhof,⁸⁹ a 500 eV plane wave energy cutoff, and uniform k -meshes with k -point density ≥ 700 k -points/Å⁻³. The energy and ionic forces are converged to within 10⁻⁶ eV and 0.01 eV/Å, respectively. Lattice dynamical properties are computed using PHONOPY⁹⁰ with approximately cubic supercells^{91,92} of 216 atoms for $\text{Cu}_2\text{AgBiPbS}_4$ and 200 atoms for $\text{MnTl}_2\text{As}_2\text{S}_5$. We use atomic displacements of 0.005 Å to compute the phonons and volume differences of $\pm 1.5\%$ to compute the mode Grüneisen parameter. κ_L is computed via the Debye-Callaway model^{77–79} and compared to the minimum (amorphous limit) values.⁸² The reciprocal space high-symmetry paths are based on Ref. 93.

Acknowledgement We acknowledge support from the U.S. Department of Energy under Contract de-sc0014520 (lattice dynamical calculations) and Toyota Research Institute through the Accelerated Materials Design and Discovery program (materials design). Computational resources were provided by the National Energy Research Scientific Computing Center (U.S. Department of Energy Contract DE-AC02-05CH11231), the Extreme Science and Engineering Discovery Environment (National Science Foundation Contract ACI-1548562), and the Quest high performance computing facility at Northwestern University.

Supporting Information Available

The following files are available free of charge. Full list and characterization of the identified compounds, screening criteria details, results and discussion of dynamical instability in $\text{Cu}_2\text{AgBiPbS}_4$, acoustic branch definitions and visualization of phonon modes of $\text{Cu}_2\text{AgBiPbS}_4$ and $\text{MnTl}_2\text{As}_2\text{S}_5$, and calculations of electronic properties and coupling with anharmonic phonons of $\text{Cu}_2\text{AgBiPbS}_4$ and $\text{MnTl}_2\text{As}_2\text{S}_5$.

References

- (1) Goldsmid, H. J. *Introduction to Thermoelectricity*; Springer Series in Materials Science; Springer: Berlin, Heidelberg, 2010; Vol. 121.
- (2) Snyder, G. J.; Toberer, E. S. Complex thermoelectric materials. *Nat. Mater.* **2008**, *7*, 105–114.
- (3) Majumdar, A. Thermoelectricity in Semiconductor Nanostructures. *Science* **2004**, *303*, 777–778.
- (4) Poudel, B.; Hao, Q.; Ma, Y.; Lan, Y.; Minnich, A.; Yu, B.; Yan, X.; Wang, D.; Muto, A.; Vashaee, D. et al. High-Thermoelectric Performance of Nanostructured Bismuth Antimony Telluride Bulk Alloys. *Science* **2008**, *320*, 634–638.
- (5) Minnich, A. J.; Dresselhaus, M. S.; Ren, Z. F.; Chen, G. Bulk nanostructured thermoelectric materials: current research and future prospects. *Energy Environ. Sci.* **2009**, *2*, 466–479.
- (6) Vineis, C. J.; Shakouri, A.; Majumdar, A.; Kanatzidis, M. G. Nanostructured Thermoelectrics: Big Efficiency Gains from Small Features. *Adv. Mater.* **2010**, *22*, 3970–3980.
- (7) Garg, J.; Bonini, N.; Kozinsky, B.; Marzari, N. Role of Disorder and Anharmonicity in the Thermal Conductivity of Silicon-Germanium Alloys: A First-Principles Study. *Phys. Rev. Lett.* **2011**, *106*, 045901.
- (8) Biswas, K.; He, J.; Blum, I. D.; Wu, C.-I.; Hogan, T. P.; Seidman, D. N.; Dravid, V. P.; Kanatzidis, M. G. High-performance bulk thermoelectrics with all-scale hierarchical architectures. *Nature* **2012**, *489*, 414–418.
- (9) Tian, Z.; Garg, J.; Esfarjani, K.; Shiga, T.; Shiomi, J.; Chen, G. Phonon conduction in PbSe, PbTe, and $\text{PbTe}_{1-x}\text{Se}_x$ from first-principles calculations. *Phys. Rev. B* **2012**, *85*, 184303.
- (10) Hori, T.; Shiga, T.; Shiomi, J. Phonon transport analysis of silicon germanium alloys using molecular dynamics simulations. *J. Appl. Phys.* **2013**, *113*, 203514.
- (11) Shiga, T.; Hori, T.; Shiomi, J. Influence of mass contrast in alloy phonon scattering. *Jpn. J. Appl. Phys.* **2014**, *53*, 021802.
- (12) Lindsay, L.; Hua, C.; Ruan, X. L.; Lee, S. Survey of ab initio phonon thermal transport. *Mater. Today Phys.* **2018**, *7*, 106–120.
- (13) Hao, S.; Dravid, V. P.; Kanatzidis, M. G.; Wolverton, C. Computational strategies for design and discovery of nanostructured thermoelectrics. *npj Comput. Mater.* **2019**, *5*, 1–10.
- (14) Jana, M. K.; Biswas, K. Crystalline Solids with Intrinsically Low Lattice Thermal Conductivity for Thermoelectric Energy Conversion. *ACS Energy Lett.* **2018**, *3*, 1315–1324.
- (15) IUPAC - lone (electron) pair. <https://goldbook.iupac.org/terms/view/L03618>, accessed 1/21/2020.
- (16) Greenwood, N. N.; Earnshaw, A. *Chemistry of the Elements 2nd Edition*; Butterworth-Heinemann, 1997.

- (17) Seshadri, R.; Hill, N. A. Visualizing the Role of Bi 6s “Lone Pairs” in the Off-Center Distortion in Ferromagnetic BiMnO₃. *Chem. Mater.* **2001**, *13*, 2892–2899.
- (18) Waghmare, U. V.; Spaldin, N. A.; Kandpal, H. C.; Seshadri, R. First-principles indicators of metallicity and cation off-centricity in the IV-VI rocksalt chalcogenides of divalent Ge, Sn, and Pb. *Phys. Rev. B* **2003**, *67*, 125111.
- (19) Stoltzfus, M. W.; Woodward, P. M.; Seshadri, R.; Klepeis, J.-H.; Bursten, B. Structure and Bonding in SnWO₄, PbWO₄, and BiVO₄: Lone Pairs vs Inert Pairs. *Inorg. Chem.* **2007**, *46*, 3839–3850.
- (20) Walsh, A.; J. Payne, D.; G. Egdell, R.; W. Watson, G. Stereochemistry of post-transition metal oxides: revision of the classical lone pair model. *Chem. Soc. Rev.* **2011**, *40*, 4455–4463.
- (21) Petrov, A.; Shtrum, E. Heat Conductivity and the Chemical Bond in ABX₂-Type Compounds. *Soviet Physics-Solid state* **1962**, *4*, 1061–1065.
- (22) Morelli, D. T.; Jovovic, V.; Heremans, J. P. Intrinsically Minimal Thermal Conductivity in Cubic I-V-VI₂ Semiconductors. *Phys. Rev. Lett.* **2008**, *101*, 035901.
- (23) Skoug, E. J.; Cain, J. D.; Morelli, D. T. Structural effects on the lattice thermal conductivity of ternary antimony- and bismuth-containing chalcogenide semiconductors. *Appl. Phys. Lett.* **2010**, *96*, 181905.
- (24) Zhang, Y.; Skoug, E.; Cain, J.; Ozoliņš, V.; Morelli, D.; Wolverton, C. First-principles description of anomalously low lattice thermal conductivity in thermoelectric Cu-Sb-Se ternary semiconductors. *Phys. Rev. B* **2012**, *85*, 054306.
- (25) McGuire, M. A.; Reynolds, T. K.; DiSalvo, F. J. Exploring Thallium Compounds as Thermoelectric Materials: Seventeen New Thallium Chalcogenides. *Chem. Mater.* **2005**, *17*, 2875–2884.
- (26) Dutta, M.; Pal, K.; V. Waghmare, U.; Biswas, K. Bonding heterogeneity and lone pair induced anharmonicity resulted in ultralow thermal conductivity and promising thermoelectric properties in n-type AgPbBiSe₃. *Chem. Sci.* **2019**, *10*, 4905–4913.
- (27) Mukhopadhyay, S.; Parker, D. S.; Sales, B. C.; Puretzy, A. A.; McGuire, M. A.; Lindsay, L. Two-channel model for ultralow thermal conductivity of crystalline Tl₃VSe₄. *Science* **2018**, *360*, 1455–1458.
- (28) Dong, Y.; Khabibullin, A. R.; Wei, K.; Salvador, J. R.; Nolas, G. S.; Woods, L. M. Bournonite PbCuSbS₃: Stereochemically Active Lone-Pair Electrons that Induce Low Thermal Conductivity. *ChemPhysChem* **2015**, *16*, 3264–3270.
- (29) Zhao, L.-D.; He, J.; Berardan, D.; Lin, Y.; Li, J.-F.; Nan, C.-W.; Dragoe, N. BiCuSeO oxyselenides: new promising thermoelectric materials. *Energy Environ. Sci.* **2014**, *7*, 2900–2924.
- (30) Du, B.; Zhang, R.; Chen, K.; Mahajan, A.; Reece, M. J. The impact of lone-pair electrons on the lattice thermal conductivity of the thermoelectric compound CuSbS₂. *J. Mater. Chem. A* **2017**, *5*, 3249–3259.
- (31) Chetty, R.; Bali, A.; C. Mallik, R. Tetrahedrites as thermoelectric materials: an overview. *J. Mater. Chem. C* **2015**, *3*, 12364–12378.
- (32) Zhang, R.-z.; Chen, K.; Du, B.; Reece, M. J. Screening for Cu-S based thermoelectric materials using crystal structure features. *J. Mater. Chem. A* **2017**, *5*, 5013–5019.

- (33) Skoug, E. J.; Morelli, D. T. Role of Lone-Pair Electrons in Producing Minimum Thermal Conductivity in Nitrogen-Group Chalcogenide Compounds. *Phys. Rev. Lett.* **2011**, *107*, 235901.
- (34) Wang, X.; Liebau, F. Studies on bond and atomic valences. I. correlation between bond valence and bond angles in Sb^{III} chalcogen compounds: the influence of lone-electron pairs. *Acta Crystallogr. B* **1996**, *52*, 7–15.
- (35) Wang, H.; Qin, G.; Qin, Z.; Li, G.; Wang, Q.; Hu, M. Lone-Pair Electrons Do Not Necessarily Lead to Low Lattice Thermal Conductivity: An Exception of Two-Dimensional Penta-CN₂. *J. Phys. Chem. Lett.* **2018**, *9*, 2474–2483.
- (36) Zunger, A. Inverse design in search of materials with target functionalities. *Nat Rev. Chem.* **2018**, *2*, 0121.
- (37) Isaacs, E. B.; Wolverton, C. Inverse Band Structure Design via Materials Database Screening: Application to Square Planar Thermoelectrics. *Chem. Mater.* **2018**, *30*, 1540–1546.
- (38) Isaacs, E. B.; Wolverton, C. Materials Informatics Approach to the Identification of One-Band Correlated Materials Analogous to the Cuprates. *Phys. Rev. X* **2019**, *9*, 021042.
- (39) Saal, J. E.; Kirklin, S.; Aykol, M.; Meredig, B.; Wolverton, C. Materials Design and Discovery with High-Throughput Density Functional Theory: The Open Quantum Materials Database (OQMD). *JOM* **2013**, *65*, 1501–1509.
- (40) Kirklin, S.; Saal, J. E.; Meredig, B.; Thompson, A.; Doak, J. W.; Aykol, M.; Rühl, S.; Wolverton, C. The Open Quantum Materials Database (OQMD): assessing the accuracy of DFT formation energies. *npj Comput. Mater.* **2015**, *1*, 15010.
- (41) Hohenberg, P.; Kohn, W. Inhomogeneous Electron Gas. *Phys. Rev.* **1964**, *136*, B864–B871.
- (42) Kohn, W.; Sham, L. J. Self-Consistent Equations Including Exchange and Correlation Effects. *Phys. Rev.* **1965**, *140*, A1133–A1138.
- (43) Bergerhoff, G.; Hundt, R.; Sievers, R.; Brown, I. D. The inorganic crystal structure data base. *J. Chem. Inf. Comput. Sci.* **1983**, *23*, 66–69.
- (44) Belsky, A.; Hellenbrandt, M.; Karen, V. L.; Luksch, P. New developments in the Inorganic Crystal Structure Database (ICSD): accessibility in support of materials research and design. *Acta Crystallogr. B* **2002**, *58*, 364–369.
- (45) Sun, W.; Dacek, S. T.; Ong, S. P.; Hautier, G.; Jain, A.; Richards, W. D.; Gamst, A. C.; Persson, K. A.; Ceder, G. The thermodynamic scale of inorganic crystalline metastability. *Sci. Adv.* **2016**, *2*, e1600225.
- (46) Hoppe, R. Effective coordination numbers (ECoN) and mean fictive ionic radii (MEFIR). *Z. Kristallogr. Cryst. Mater.* **1979**, *150*, 23–52.
- (47) Guin, S. N.; Biswas, K. Cation Disorder and Bond Anharmonicity Optimize the Thermoelectric Properties in Kinetically Stabilized Rocksalt AgBiS₂ Nanocrystals. *Chem. Mater.* **2013**, *25*, 3225–3231.
- (48) Kim, J.-H.; Chung, D.-Y.; Bile, D.; Loo, S.; Short, J.; Mahanti, S. D.; Hogan, T.; Kanatzidis, M. G. Crystal Growth, Thermoelectric Properties, and Electronic Structure of AgBi₃S₅ and AgSb_xBi_{3-x}S₅ ($x = 0.3$). *Chem. Mater.* **2005**, *17*, 3606–3614.
- (49) Tan, G.; Hao, S.; Zhao, J.; Wolverton, C.; Kanatzidis, M. G. High Thermoelectric Performance in Electron-Doped AgBi₃S₅

- with Ultralow Thermal Conductivity. *J. Am. Chem. Soc.* **2017**, *139*, 6467–6473.
- (50) Hor, Y. S.; Richardella, A.; Roushan, P.; Xia, Y.; Checkelsky, J. G.; Yazdani, A.; Hasan, M. Z.; Ong, N. P.; Cava, R. J. *p*-type Bi₂Se₃ for topological insulator and low-temperature thermoelectric applications. *Phys. Rev. B* **2009**, *79*, 195208.
- (51) Parker, D.; Singh, D. J. Potential Thermoelectric Performance from Optimization of Hole-Doped Bi₂Se₃. *Phys. Rev. X* **2011**, *1*, 021005.
- (52) Heremans, J. P.; Cava, R. J.; Samarth, N. Tetradymites as thermoelectrics and topological insulators. *Nat. Rev. Mater.* **2017**, *2*, 1–21.
- (53) Pei, Y.; Chang, C.; Wang, Z.; Yin, M.; Wu, M.; Tan, G.; Wu, H.; Chen, Y.; Zheng, L.; Gong, S. et al. Multiple Converged Conduction Bands in K₂Bi₈Se₁₃: A Promising Thermoelectric Material with Extremely Low Thermal Conductivity. *J. Am. Chem. Soc.* **2016**, *138*, 16364–16371.
- (54) Pan, L.; Bérardan, D.; Dragoe, N. High Thermoelectric Properties of n-Type AgBiSe₂. *J. Am. Chem. Soc.* **2013**, *135*, 4914–4917.
- (55) Witting, I. T.; Chasapis, T. C.; Ricci, F.; Peters, M.; Heinz, N. A.; Hautier, G.; Snyder, G. J. The Thermoelectric Properties of Bismuth Telluride. *Adv. Electron. Mater.* **2019**, *5*, 1800904.
- (56) Tian, Y.; Jia, S.; Cava, R. J.; Zhong, R.; Schneeloch, J.; Gu, G.; Burch, K. S. Understanding the evolution of anomalous anharmonicity in Bi₂Te_{3-x}Se_x. *Phys. Rev. B* **2017**, *95*, 094104.
- (57) Irie, T.; Takahama, T.; Ono, T. The Thermoelectric Properties of AgSbTe₂–AgBiTe₂, AgSbTe₂–PbTe and–SnTe Systems. *Jpn. J. Appl. Phys.* **1963**, *2*, 72.
- (58) Tan, G.; Shi, F.; Sun, H.; Zhao, L.-D.; Uher, C.; Dravid, V. P.; Kanatzidis, M. G. SnTe–AgBiTe₂ as an efficient thermoelectric material with low thermal conductivity. *J. Mater. Chem. A* **2014**, *2*, 20849–20854.
- (59) Kuznetsova, L. A.; Kuznetsov, V. L.; Rowe, D. M. Thermoelectric properties and crystal structure of ternary compounds in the Ge(Sn,Pb)Te–Bi₂Te₃ systems. *J. Phys. Chem. Solids* **2000**, *61*, 1269–1274.
- (60) Shelimova, L. E.; Karpinskii, O. G.; Zemskov, V. S.; Konstantinov, P. P. Structural and electrical properties of layered tetradymite-like compounds in the GeTe–Bi₂Te₃ and GeTe–Sb₂Te₃ systems. *Inorg. Mater.* **2000**, *36*, 235–242.
- (61) Kuznetsov, V. L.; Kuznetsova, L. A.; Rowe, D. M. Effect of nonstoichiometry on the thermoelectric properties of GeBi₄Te₇. *J. Appl. Phys.* **1999**, *85*, 3207–3210.
- (62) Shelimova, L. E.; Karpinskii, O. G.; Konstantinov, P. P.; Avilov, E. S.; Kretova, M. A.; Zemskov, V. S. Crystal Structures and Thermoelectric Properties of Layered Compounds in the ATe–Bi₂Te₃ (A = Ge, Sn, Pb) Systems. *Inorg. Mater.* **2004**, *40*, 451–460.
- (63) Wölfling, B.; Kloc, C.; Teubner, J.; Bucher, E. High Performance Thermoelectric Tl₉BiTe₆ with an Extremely Low Thermal Conductivity. *Phys. Rev. Lett.* **2001**, *86*, 4350–4353.
- (64) Yamanaka, S.; Kosuga, A.; Kurosaki, K. Thermoelectric properties of Tl₉BiTe₆. *J. Alloys Compd.* **2003**, *352*, 275–278.
- (65) Kurosaki, K.; Kosuga, A.; Muta, H.; Yamanaka, S. Thermoelectric Properties of Thallium Compounds with Extremely Low Thermal Conductivity. *Mater. Trans.* **2005**, *46*, 1502–1505.
- (66) Guo, Q.; Chan, M.; Kuropatwa, B. A.; Kleinke, H. Enhanced Thermoelectric Properties of Variants of Tl₉SbTe₆ and

- Tl₉BiTe₆. *Chem. Mater.* **2013**, *25*, 4097–4104.
- (67) Tyagi, K.; Gahtori, B.; Bathula, S.; Srivastava, A. K.; Shukla, A. K.; Auluck, S.; Dhar, A. Thermoelectric properties of Cu₃SbSe₃ with intrinsically ultralow lattice thermal conductivity. *J. Mater. Chem. A* **2014**, *2*, 15829–15835.
- (68) Tyagi, K.; Gahtori, B.; Bathula, S.; Toutam, V.; Sharma, S.; Singh, N. K.; Dhar, A. Thermoelectric and mechanical properties of spark plasma sintered Cu₃SbSe₃ and Cu₃SbSe₄: Promising thermoelectric materials. *Appl. Phys. Lett.* **2014**, *105*, 261902.
- (69) Wang, H.; Li, J.-F.; Zou, M.; Sui, T. Synthesis and transport property of AgSbTe₂ as a promising thermoelectric compound. *Appl. Phys. Lett.* **2008**, *93*, 202106.
- (70) Jovovic, V.; Heremans, J. P. Measurements of the energy band gap and valence band structure of AgSbTe₂. *Phys. Rev. B* **2008**, *77*, 245204.
- (71) Kurosaki, K.; Uneda, H.; Muta, H.; Yamanaka, S. Thermoelectric properties of thallium antimony telluride. *J. Alloys Compd.* **2004**, *376*, 43–48.
- (72) Topa, D.; Makovicky, E.; Putz, H. The Crystal Structure of Angelaite, Cu₂AgPbBiS₄. *Can. Mineral.* **2010**, *48*, 145–153.
- (73) Gostojić, M.; Edenharter, A.; Nowacki, W.; Engel, P. The crystal structure of synthetic Tl₂MnAs₂S₅. *Z. Kristallogr. Cryst. Mater.* **1982**, *158*, 43–51.
- (74) Nowacki, W.; Edenharter, A.; Engel, P.; Gostojić, M.; Nagl, A. On the Crystal Chemistry of Some Thallium Sulphides and Sulphosalts. *Ore Genesis*. Berlin, Heidelberg, 1982; pp 689–704.
- (75) Christensen, M.; Abrahamsen, A. B.; Christensen, N. B.; Juranyi, F.; Andersen, N. H.; Lefmann, K.; Andreasson, J.; Bahl, C. R. H.; Iversen, B. B. Avoided crossing of rattler modes in thermoelectric materials. *Nat. Mater.* **2008**, *7*, 811–815.
- (76) Toberer, E. S.; Zevalkink, A.; Snyder, G. J. Phonon engineering through crystal chemistry. *J. Mater. Chem.* **2011**, *21*, 15843–15852.
- (77) Callaway, J. Model for Lattice Thermal Conductivity at Low Temperatures. *Phys. Rev.* **1959**, *113*, 1046–1051.
- (78) Morelli, D. T.; Heremans, J. P.; Slack, G. A. Estimation of the isotope effect on the lattice thermal conductivity of group IV and group III-V semiconductors. *Phys. Rev. B* **2002**, *66*, 195304.
- (79) Zhang, Y. First-principles Debye–Callaway approach to lattice thermal conductivity. *J. Materiomics* **2016**, *2*, 237–247.
- (80) Tan, G.; Shi, F.; Hao, S.; Zhao, L.-D.; Chi, H.; Zhang, X.; Uher, C.; Wolverton, C.; Dravid, V. P.; Kanatzidis, M. G. Non-equilibrium processing leads to record high thermoelectric figure of merit in PbTe–SrTe. *Nat. Commun.* **2016**, *7*, 1–9.
- (81) Zhao, J.; Hao, S.; Islam, S. M.; Chen, H.; Ma, S.; Wolverton, C.; Kanatzidis, M. G. Quaternary Chalcogenide Semiconductors with 2D Structures: Rb₂ZnBi₂Se₅ and Cs₆Cd₂Bi₈Te₁₇. *Inorg. Chem.* **2018**, *57*, 9403–9411.
- (82) Cahill, D. G.; Watson, S. K.; Pohl, R. O. Lower limit to the thermal conductivity of disordered crystals. *Phys. Rev. B* **1992**, *46*, 6131–6140.
- (83) Nielsen, M. D.; Ozoliņš, V.; Heremans, J. P. Lone pair electrons minimize lattice thermal conductivity. *Energy Environ. Sci.* **2013**, *6*, 570–578.

- (84) Tolborg, K.; Gatti, C.; Iversen, B. B. Expression and interactions of stereochemically active lone pairs and their relation to structural distortions and thermal conductivity. *arXiv:2002.01459*.
- (85) Blöchl, P. E. Projector augmented-wave method. *Phys. Rev. B* **1994**, *50*, 17953–17979.
- (86) Kresse, G.; Joubert, D. From ultrasoft pseudopotentials to the projector augmented-wave method. *Phys. Rev. B* **1999**, *59*, 1758–1775.
- (87) Recommended PAW potentials for DFT calculations using vasp.5.2. https://cms.mpi.univie.ac.at/vasp/vasp/Recommended_PAW_potentials_DFT_calculations_using_vasp_5_2.html, Accessed: 2019-09-01.
- (88) Kresse, G.; Furthmüller, J. Efficiency of ab-initio total energy calculations for metals and semiconductors using a plane-wave basis set. *Comput. Mater. Sci.* **1996**, *6*, 15–50.
- (89) Perdew, J. P.; Burke, K.; Ernzerhof, M. Generalized Gradient Approximation Made Simple. *Phys. Rev. Lett.* **1996**, *77*, 3865–3868.
- (90) Togo, A.; Oba, F.; Tanaka, I. First-principles calculations of the ferroelastic transition between rutile-type and CaCl₂-type SiO₂ at high pressures. *Phys. Rev. B* **2008**, *78*, 134106.
- (91) Erhart, P.; Sadigh, B.; Schleife, A.; Åberg, D. First-principles study of codoping in lanthanum bromide. *Phys. Rev. B* **2015**, *91*, 165206.
- (92) Larsen, A. H.; Mortensen, J. J.; Blomqvist, J.; Castelli, I. E.; Christensen, R.; Dułak, M.; Friis, J.; Groves, M. N.; Hammer, B.; Hargus, C. et al. The atomic simulation environment—a Python library for working with atoms. *J. Phys. Condens. Matter* **2017**, *29*, 273002.
- (93) Setyawan, W.; Curtarolo, S. High-throughput electronic band structure calculations: Challenges and tools. *Comput. Mater. Sci.* **2010**, *49*, 299–312.